Research Square

Preprints are preliminary reports that have not undergone peer review.
They should not be considered conclusive, used to inform clinical practice,
or referenced by the media as validated information.

Signal propagation and separation in a self-organized three-dimensional neural network with activity-dependent conduction

Victor Trubitsin

tvy@udman.ru

Udmurt Federal Research Center, Ural Branch of the Russian Academy of Sciences

Research Article

Keywords: Spiking neural network, Activity-dependent myelination, Conduction delay, Short-term synaptic depression, Signal pathway, Community detection

Posted Date: November 12th, 2026

DOI: https://doi.org/10.21203/rs.3.rs-11535023/v1

License: This work is licensed under a Creative Commons Attribution 4.0 International License.
Read Full License

Additional Declarations: No competing interests reported.

Signal propagation and separation in a self-organized three-dimensional neural network with activity-dependent conduction

V. Yu. Trubitsin[1*]

[1*]Udmurt Federal Research Center, Ural Branch of the Russian Academy of Sciences, 34 T. Baramzinoy St., Izhevsk, 426067, Russia.

Corresponding author(s). E-mail(s): tvy@udman.ru;

Abstract

Activity-dependent myelination makes conduction delays and connection strengths depend on the history of transmitted signals, but how this shapes signal propagation in spatially embedded networks is poorly understood. We study spike propagation in three-dimensional neural networks grown by an energy-based self-organization model. The delay of a connection is set by the lengths and thicknesses of the axon and the dendrite, and its weight by the thinner of the two and by dendritic attenuation; thickness grows with passing spikes up to a maximum and decays without them, and short-term synaptic depression limits transmission. In networks of 100–500 neurons, the transition from local activity to activation of the whole network is sharp as the connection weight increases. Without depression, thickness plasticity drives self-sustained activity, and a dimensionless synaptic load separates a relay regime from an onset-detector regime. We propose to extract the signal pathway from the growth of connection weights and introduce measures for comparing pathways: pathways from different inputs barely overlap, and nested stimuli produce nested pathways. Community detection by modularity maximization does not recover the signal pathway, because the pathway is an elongated tree rather than a dense group; we also show that the spatial null model of modularity must be normalized. Comparison with random networks built without growth shows that growth makes connections local, and a random network whose connection probability decays with distance as in the grown network and whose axon capacity is limited reproduces the functional properties of the grown network.

Keywords: Spiking neural network, Activity-dependent myelination, Conduction delay, Short-term synaptic depression, Signal pathway, Community detection

1 Introduction

We have developed an energy-based model of self-organization of a system of identical neuron-like particles: axons and dendrites grow along the gradient of the total field created by neurons, axons and dendrites, and a connection forms when a dendrite end approaches an axon end (the growth rules used in this work are described in Section 2). To analyse the resulting three-dimensional network, the Louvain method was adapted with spatial attenuation in the modularity (Trubitsin 2026). The growth model and the Louvain method describe the *structure* of the network. Connectome generative models address a related problem: they reproduce statistical properties of brain networks from simple rules such as the distance between neurons, cell types and synaptic pruning (Richter and Schneidman 2025), including models with explicit axon growth: in Liu et al. (2024) the axon tip moves step by step along the net attractive force towards the nodes, which decays with distance. This principle is close to our growth model but is applied to brain regions in a plane. These studies compare structural properties of networks and do not model signal propagation through them. The next natural question is how a signal propagates through the grown network and how the passage of the signal in turn reshapes the network.

In the nervous system, conduction velocity along an axon increases with its diameter and degree of myelination: for myelinated fibres it is approximately proportional to the diameter (Hursh 1939), and for unmyelinated fibres and dendrites to the square root of the diameter. Myelination is activity-dependent: frequently used axons become more myelinated, which changes conduction delays and signal synchrony (Fields 2015; Pajevic et al. 2014; Bonetto et al. 2021). In computational models, activity-dependent adjustment of conduction velocity stabilizes synchronous oscillations in large-scale brain networks (Noori et al. 2020) and acts as a homeostatic mechanism that enhances the firing rates and correlations of a spiking network (Talidou et al. 2022). If an oligodendrocyte responds to spikes in all the axons it myelinates, such adjustment selectively synchronizes correlated spike trains (Pajevic et al. 2023). As noted in a review of such models (Nguyen and Lefebvre 2026), activity in them changes only the conduction velocity, while synaptic connections and their weights remain fixed. Activity also changes the connections themselves: frequently used synapses are strengthened and unused ones weaken (Hebb 1949; Butz et al. 2009); in models with spike-timing dependent plasticity this gives rise to neuronal assemblies (Litwin-Kumar and Doiron 2014). Finally, frequent stimulation of a synapse depletes its transmitter supply (short-term depression (Tsodyks and Markram 1997)), which limits the transmission of high-frequency signals and changes the regimes of network dynamics, up to periodic bursting and bistability (Gast et al. 2021).

Community detection by modularity maximization (Newman and Girvan 2004; Blondel et al. 2008; Fortunato 2010) is widely used to identify functionally related groups of neurons, including detection based on spiking activity (Humphries 2011; Shimono and Beggs 2015) and with spatial null models that account for the distance between nodes (Expert et al. 2011; Betzel et al. 2017). Modularity looks for groups in which connections are denser than expected. However, the trace that a passing signal leaves in the network need not be a dense group: the signal travels along chains of

connections from inputs to outputs, and it is not obvious whether community detection can recover such a trace.

In this work we study spike propagation in self-organized three-dimensional networks grown by the energy-based model, with delays determined by the geometry and thickness of axons and dendrites and with activity-dependent changes of thickness. To this end we build a model in which the length and thickness of the axon and the dendrite set both the delay and the weight of a connection, while thickness changes under the action of passing spikes. We examine under what conditions the signal spreads over the network and what role transmitter depletion plays in this. We then propose a way to extract the signal pathway from changes in connection weights and to compare pathways evoked by different stimuli, and test whether such a pathway can be found by community detection based on modularity maximization. Finally, we compare the grown networks with random networks built without growth to find out which properties of signal propagation are determined by growth itself.

2 Model

The network through which the signal propagates is grown by the energy-based growth model in the unit cube $[0, 1]^3$. All lengths in the model are dimensionless and measured in units of the domain size L_{dom} ($L_{\mathrm{dom}} = 1$ mm in the simulations), and conduction velocities in L_{dom}/ms, so that for $L_{\mathrm{dom}} = 1$ mm a velocity of 1 m/s equals one. Neuron i is given by its centre $\mathbf{r}_i$, and its axons and dendrites by segments from the centre to their ends $\mathbf{a}$ and $\mathbf{e}$, respectively. Some neurons are designated as input neurons (placed near one face of the domain) and output neurons (near the opposite face); the dendrites of input neurons do not grow and receive the external signal, and the axons of output neurons do not move. Axons grow along the gradient of the total field of neurons, axons and dendrites, then dendrites grow towards axons, and a connection forms when a dendrite end comes within the capture radius of an axon end. The model uses an absorption radius of energy by dendrites, normalization of the fields by the number of sources, and a limited growth step of axons with termination by the largest displacement; these details affect the network structure quantitatively but not qualitatively. A limited *axon capacity* turned out to be essential. A dendrite end moves along the gradient of the field created by the ends of all axons, and without a limit the dendrites gather at a few axons: for $N = 300$–500, up to 20 dendrites attach to a single axon and 28–35 % of axons are not caught by any dendrite (with a random distribution of two dendrites per axon on average this would be about 13 %). Neurons with an uncaught axon do not pass the signal on, and if such a neuron is an input neuron, its signal does not enter the network. Therefore the contribution of an axon to the dendrite growth field is divided by $1 + n$, where n is the number of dendrites already attached to it: an occupied axon attracts new dendrites more weakly. This rule introduces no new parameters, reduces the fraction of uncaught axons to 4–7 % and the largest number of dendrites per axon to 6–12, while the lengths of axons and dendrites remain practically unchanged. Axons grow in a field that includes attraction to neurons, repulsion from them at short distances, and repulsion from other axons.

The initial state is random: neuron centres are uniformly distributed in the cube, the end of each axon is placed at a random point of the cube, and the end of each dendrite at a random point at a distance between 0.05 and 0.2 from the centre of its neuron. Axon growth is characterized by the *total energy* of the network, the sum of the axon field and the neuron field at axon ends:

$$E = \sum_k \big[\Phi_A(\mathbf{a}_k) + \Phi_N(\mathbf{a}_k)\big],$$
$$\Phi_A(\mathbf{r}) = \frac{E_A}{N_A}\sum_l e^{-\alpha_A|\mathbf{r}-\mathbf{a}_l|}, \quad \Phi_N(\mathbf{r}) = \frac{E_N}{N}\sum_i e^{-\alpha_N|\mathbf{r}-\mathbf{r}_i|}, \tag{1}$$

where the sums run over axon ends $\mathbf{a}_l$ and neuron centres $\mathbf{r}_i$ (excluding points that coincide with $\mathbf{r}$), N_A is the number of axons, $E_A = E_N = 1000$ are the axon and neuron energies, and $\alpha_A = 40$ and $\alpha_N = 15$ are the field attenuation coefficients. Axon ends move up the field gradient, so E increases during growth; this quantity is reported by the program during growth. The energy (1) depends only on the positions of axon ends and neurons and does not depend on which dendrites are attached to the axons. The result of growth is a directed graph embedded in space: each connection has not only a source and a target but also a geometry, namely the lengths of the axon and dendrite along which the signal travels.

We call the elementary unit of transmission a *contact*: contact $i \to j$ is a dendrite of neuron j that has caught an axon of neuron i. A spike emitted by neuron i travels along the axon from the centre to its end, crosses the synaptic gap to the dendrite end, and travels along the dendrite to the centre of neuron j (Fig. 1). The lengths of these segments,

$$L_a = |\mathbf{a} - \mathbf{r}_i|, \qquad L_d = |\mathbf{e} - \mathbf{r}_j|,$$

are measured in domain units. If neuron i has several axons, the one whose end is closest to the dendrite end is used; unconnected dendrites do not conduct. A pair of neurons may share several contacts (through different dendrites), which act independently.

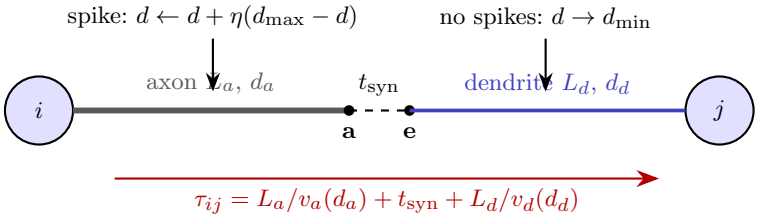


Fig. 1 Scheme of contact $i \to j$: the spike path along the axon, across the synaptic gap and along the dendrite; the red arrow is the total delay τ_{ij}; the upper labels show the change of thickness (see text).

The neuron is modelled as a leaky integrate-and-fire (LIF) unit (Gerstner and Kistler 2002; Burkitt 2006). This is the simplest model that retains the two properties essential for our problem: summation of incoming spikes and a firing threshold.

Between inputs the membrane potential V decays to the resting potential V_{rest} with time constant τ_m, $\tau_m \dot{V} = -(V - V_{\mathrm{rest}})$, and each incoming spike increases V by the weight w of the contact through which it arrived. When V reaches the threshold θ, the neuron fires (emits a spike), the potential is reset to V_{reset}, and inputs are ignored during the refractory period t_{ref}. The equation is integrated with step Δt using a scheme exact for exponential decay:

$$V_{s+1} = V_{\mathrm{rest}} + (V_s - V_{\mathrm{rest}})\, e^{-\Delta t/\tau_m} + I_s,$$

where V_s is the potential at step s and I_s is the sum of the weights of spikes arriving at that step. With $\tau_m = 5$ ms the neuron "forgets" its input within a few milliseconds and fires only if spikes from several neighbours arrive almost simultaneously; conduction delays, which are of the same order in the grown network, therefore determine which neurons fire.

The contact delay is determined by the conduction velocity along the axon and dendrite. In the nervous system the velocity increases with fibre diameter: for myelinated axons it is approximately proportional to the diameter (Hursh 1939; Rushton 1951), and for unmyelinated fibres and dendrites, according to cable theory, to the square root of the diameter (Rushton 1951; Rall 1962). Generalizing both cases, we set

$$v(d) = v_0 \Big(\frac{d}{d_0}\Big)^{\beta}, \tag{2}$$

where d is the current thickness (in arbitrary units), d_0 the initial thickness, v_0 the velocity at $d = d_0$, and β an exponent: $\beta = 1$ for axons and $\beta = \frac{1}{2}$ for dendrites. The delay of contact $i \to j$ is then

$$\tau_{ij} = \frac{L_a}{v_a(d_a)} + t_{\mathrm{syn}} + \frac{L_d}{v_d(d_d)}, \tag{3}$$

where v_a and v_d are the velocities (2) with axon and dendrite parameters, d_a and d_d their thicknesses, and t_{syn} the synaptic delay, which also includes crossing the gap between the axon and dendrite ends. Since lengths are measured in L_{dom} and velocities in L_{dom}/ms, the delay is in ms. For typical values (Table A1 in Appendix A) an axon of mean length 0.65 is traversed in 0.65 ms and a dendrite of length 0.21 in 1 ms, so $\tau_{ij} \approx 2$ ms, comparable to τ_m. Thickening to $d_{\max} = 3$ shortens the axonal conduction time threefold and the dendritic time by a factor of $\sqrt{3}$. The role of delays in forming precisely synchronized groups of neurons was shown in (Izhikevich 2006), and the link between myelin plasticity and synchrony in Pajevic et al. (2014).

The contact weight, i.e., the jump in the potential of neuron j caused by one spike, is the product of two factors:

$$w_{ij} = w_0 \,\frac{\min(d_a, d_d)}{\min(d_{0a}, d_{0d})}\, \exp\Big(-\frac{L_d}{\lambda_0 \sqrt{d_d/d_{0d}}}\Big). \tag{4}$$

The first reflects a "bottleneck" principle: the transmitted signal is limited by the thinner of the axon and the dendrite; d_{0a} and d_{0d} are the initial thicknesses of the

axon and dendrite, so the factor equals one at initial thicknesses. The second describes passive attenuation along the dendrite with length constant $\lambda = \lambda_0\sqrt{d_d/d_{0d}}$, which according to cable theory grows as the square root of the diameter (Rall 1962); λ_0 is the length constant at initial thickness (in domain units). With $\lambda_0 = 0.5$ and a mean dendrite length of 0.21 the attenuation is $e^{-0.42} \approx 0.66$. The parameter w_0 is the contact weight at initial thicknesses and zero dendrite length; it is the main control parameter of the model, and its choice is discussed in Section 3.

Technically, a spike sent by neuron i at step s is written into the ring buffer of neuron j at step $s + \max(1, \mathrm{round}(\tau_{ij}/\Delta t))$ together with the weight w_{ij} computed at the moment of sending. Since thicknesses change slowly, delays and weights of all contacts are recomputed from the current thicknesses not at every step but once every N_{upd} steps.

The central assumption of the model is that the thickness of axons and dendrites depends on the signal passing through them. Its biological basis is activity-dependent myelination: electrical activity of axons stimulates oligodendrocyte formation and thickening of the myelin sheath, and frequently used pathways conduct faster (Gibson et al. 2014; Fields 2015; Bonetto et al. 2021); more generally, it is structural plasticity, in which used connections are reinforced and unused ones disappear (Butz et al. 2009). A similar rule was used in Talidou et al. (2022): the conduction velocity of an axon increases when its neuron fires often and decreases when it fires rarely. There, however, as in Noori et al. (2020), activity changes only the delay, whereas in our model thickness determines both the delay and the weight of a connection. We use the simplest saturating rule: each axon and dendrite has thickness $d \in [d_{\min}, d_{\max}]$, and

$$d \leftarrow d + \eta\,(d_{\max} - d) \quad \text{(at a spike)}, \qquad \frac{dd}{dt} = -\frac{d - d_{\min}}{\tau_D} \quad \text{(between spikes)}, \tag{5}$$

where $\eta \in (0, 1)$ is the fraction of the remaining margin to the maximum thickness $d_{\max}$ added by one spike, $d_{\min}$ is the thickness to which an axon or dendrite relaxes without signals, and τ_D is the relaxation time. An axon thickens every time its neuron fires, and a dendrite every time a spike is sent into its contact. The multiplicative increment guarantees $d < d_{\max}$, and relaxation to $d_{\min} < d_0$ means that unused connections weaken and slow down over time.

Rule (5) admits an exact solution for periodic spikes with period T (rate $r = 1/T$). Let $q = e^{-T/\tau_D}$ be the factor by which the excess of thickness over $d_{\min}$ decreases during one period. In the steady state the thickness just before a spike is

$$d_b = \frac{d_{\min}(1 - q) + q\,\eta\,d_{\max}}{1 - q(1 - \eta)}, \tag{6}$$

just after a spike it is $d_a = d_b + \eta(d_{\max} - d_b)$, and the period-averaged thickness is $\bar{d} = d_{\min} + (d_a - d_{\min})\frac{\tau_D}{T}(1 - q)$. For small η and $T \ll \tau_D$ the rate enters only through the dimensionless combination $x = \eta r \tau_D$, the mean number of "increments" during

the relaxation time, and

$$\bar{d} \approx d_{\min} + (d_{\max} - d_{\min}) \, \frac{x}{1+x}. \tag{7}$$

For $x \ll 1$ the thickness is close to the minimum, for $x \gg 1$ to the maximum. A connection is thicker than initially ($\bar{d} > d_0$) only for rates above the threshold

$$r_c = \frac{d_0 - d_{\min}}{d_{\max} - d_0} \cdot \frac{1}{\eta \, \tau_D}, \tag{8}$$

which for $d_0 = 1$, $d_{\min} = 0.5$, $d_{\max} = 3$, $\eta = 0.05$ equals 0.5 Hz for $\tau_D = 10$ s and 5 Hz for $\tau_D = 1$ s. Connections through which spikes pass less often than r_c become thinner, although more slowly than completely unused ones. After the signal stops, thickness decays with time constant τ_D, and the trace of activity persists in the network for a time of order τ_D; this is the "memory" of the network about the past signal, which we extract in Section 3.

Rule (5) creates positive feedback: a passing spike thickens the connection, increases its weight (up to $d_{\max}/d_0 = 3$ times) and facilitates the passage of subsequent spikes. Without a mechanism that saturates transmission, the network may switch to self-sustained activity. In real synapses such a mechanism is short-term depression, the depletion of the transmitter supply under frequent stimulation, described by the Tsodyks–Markram model (Tsodyks and Markram 1997). Each contact has a resource $R \in [0, 1]$, the available fraction of transmitter. A spike transmits weight $w_{ij}R$ and consumes a fraction U of the resource, $R \leftarrow R(1 - U)$; between spikes the resource recovers to one, $\dot{R} = (1 - R)/\tau_{\text{rec}}$, where τ_{rec} is the recovery time. Under regular spiking with rate r, the resource before a spike approaches

$$R^* = \frac{1 - e^{-1/(r\tau_{\text{rec}})}}{1 - (1-U)e^{-1/(r\tau_{\text{rec}})}} \approx \frac{1}{1 + Ur\tau_{\text{rec}}}, \tag{9}$$

(the approximation holds for $r\tau_{\text{rec}} \gg 1$). The dimensionless quantity $Ur\tau_{\text{rec}}$, the fraction of resource consumed during the recovery time, determines how much transmission is weakened: for $Ur\tau_{\text{rec}} \ll 1$ there is almost no depression, whereas for $Ur\tau_{\text{rec}} \gg 1$ the effective weight falls as $1/r$ and the weight flux through the contact, $w_{ij}R^*r$, does not exceed $w_{ij}/(U\tau_{\text{rec}})$ at any rate. As shown in Abbott et al. (1997), such synapses primarily transmit changes in the input signal; we will see that this also determines the operating regime of the whole network. Another possible limiter of activity is inhibitory neurons; the program supports them (a fraction p_{inh} of inhibitory neurons whose weights are taken with a minus sign and multiplied by g), but they are not used in this work in order not to mix the two mechanisms.

The external signal is applied to the dendrite ends of input neurons (all of them or a chosen subset): each external spike travels along the dendrite with delay $L_d/v_d(d_d)$ and contributes $w_{0,\text{in}}(d_d/d_{0d})e^{-L_d/\lambda}$ to the potential of the input neuron, where $w_{0,\text{in}}$ is the weight of the external spike. By default the thickness of input dendrites does not change, so that the input strength remains constant. We consider a periodic signal

with interval T and a Poisson signal with mean rate r. The network output is the spikes of output neurons at the moment they reach the ends of their axons.

The model is implemented in the NNBiology software package (C++, Qt). In addition, a batch utility was written for this study that grows networks with a given seed of the random number generator and performs all analysis procedures described below. A network of 500 neurons is simulated for 1 s of model time in a fraction of a second.

3 Analysis methods

The first question to be resolved in simulations is the choice of the weight w_0. As shown in Section 4, the fraction of fired neurons as a function of w_0 exhibits a sharp jump: at small weight the signal dies out near the inputs, at large weight it spreads over the whole network. The position of the jump varies from network to network, so different realizations cannot be compared at the same absolute w_0. For each network and each set of input parameters we find the threshold w_c, the smallest weight at which at least half of the neurons fire during the simulation. Since the fraction of fired neurons increases monotonically with w_0, the threshold is found by bisection on a logarithmic scale in the interval [0.02, 20] (24 steps, relative accuracy of order 10^{-6}). Simulations are then run at $w_0 = 0.97\,w_c$, just below the threshold, where activity remains local, and at $w_0 = 1.1\,w_c$, where the signal spreads over the network.

To extract the trace that the signal leaves in the network, we compare connection weights before and after the simulation. For a pair of neurons $i \to j$ let $A_{ij}(t)$ be the total weight (4) of all excitatory contacts of the pair at time t, and $g_{ij} = A_{ij}(t_{\mathrm{sim}})/A_{ij}(0)$ its growth over a simulation of length t_{sim}. For a connection not used by the signal both thicknesses relax from $d_0 = 1$ towards $d_{\min} = 0.5$, and after 2 s with $\tau_D = 10$ s $g_{ij} \approx 0.91$; for a connection through which spikes passed regularly, g_{ij} reaches 2–3. The threshold $g_0 = 1.05$ (weight increased by more than 5 %) therefore reliably separates used connections. We define the *signal pathway* as the set of connections with $g_{ij} > g_0$ that are reachable along the direction of connections from the fired input neurons, together with the neurons they connect. The reachability requirement removes connections that thickened by chance and are unrelated to the input. The pathway may contain neurons that did not fire: the signal reached them and thickened their dendrites but did not bring the potential to threshold. The pathway is thus not the set of active neurons but the change of the network caused by the signal.

Different stimuli (different groups of inputs, rates, temporal structure) leave different pathways. To compare two simulations on the same network, each starting from the initial thicknesses, we use three measures. The Jaccard indices (Jaccard 1912) over the neurons and connections of the pathways,

$$J_N = \frac{|N_1 \cap N_2|}{|N_1 \cup N_2|}, \qquad J_E = \frac{|E_1 \cap E_2|}{|E_1 \cup E_2|},$$

where N_k and E_k are the sets of pathway neurons and connections in the k-th simulation, equal one for identical pathways and zero for disjoint ones. They depend on

the choice of the threshold g_0; a smoother measure is the Pearson correlation coefficient r_g between the values of $\ln g_{ij}$ in the two simulations over all connections of the network. The logarithm is used because growth is multiplicative: doubling and halving should give contributions of equal magnitude. A value $r_g \approx 1$ means that the two stimuli change the network in the same way, $r_g \approx 0$ that the changes are independent.

Finally, the signal pathway is compared with the result of the standard approach to identifying functional groups, community detection by modularity maximization (Newman and Girvan 2004; Blondel et al. 2008; Fortunato 2010). For a directed weighted graph with connection weights W_{ij}, the modularity of a partition into communities c_i (Leicht and Newman 2008) with a spatial null model (Expert et al. 2011; Trubitsin 2026) is

$$Q = \frac{1}{m} \sum_{i,j} \Big[W_{ij} - \gamma\, P_{ij} \Big] \delta(c_i, c_j), \qquad P_{ij} = s\, \frac{k_i^{\text{out}} k_j^{\text{in}}}{m}\, f(d_{ij}), \quad f(d_{ij}) = e^{-\beta \kappa d_{ij}}. \tag{10}$$

Here $m = \sum_{ij} W_{ij}$ is the total weight, $k_i^{\text{out}} = \sum_j W_{ij}$ and $k_j^{\text{in}} = \sum_i W_{ij}$ are the out- and in-strengths of the nodes, and $\delta(c_i, c_j) = 1$ if i and j belong to the same community and 0 otherwise. P_{ij} is the expected weight of connection $i \to j$ in the null model, a random graph with the same strengths in which the connection probability decays with the distance d_{ij} between neuron centres; β is the attenuation parameter and κ a scale (as in Trubitsin 2026, coordinates are multiplied by 400, $\kappa = 1$). Modularity is positive if the weights within communities exceed the expected ones, and the resolution parameter γ (Reichardt and Bornholdt 2006) allows communities to be made coarser ($\gamma < 1$) or finer. The factor $s = m^2 / \sum_{ij} k_i^{\text{out}} k_j^{\text{in}} f(d_{ij})$ normalizes the null model so that $\sum_{ij} P_{ij} = m$, as in Expert et al. (2011); without it ($s = 1$) the expected weight is underestimated for $\beta > 0$ and Q is overestimated, which is verified in Section 4.

Communities are found by the Louvain method (Blondel et al. 2008) (20 runs with different node orderings; the partition with the largest Q is taken) for five choices of weights W_{ij}. The structural weight $S_{ij} = 1/(1 + (L_a + L_d)/10)$ (Trubitsin 2026) does not depend on the signal and, with axon and dendrite lengths of order one, is almost the same for all connections, i.e., it describes an unweighted graph. The weight after the simulation $A_{ij}(t_{\text{sim}})$, its relative growth $A/A_0 \equiv g_{ij}$ and the squared growth $(A/A_0)^2$ (which emphasizes thickened connections more strongly) reflect changes of thickness. The causal transmission weight C_{ij}, the number of spikes of neuron i after which neuron j fired within the window $[t + \tau_{ij},\ t + \tau_{ij} + 5$ ms], reflects the activity itself. The agreement of a community with the pathway (or with the set of fired neurons) is measured by $F_1 = 2PR/(P + R)$, where P is the fraction of community neurons belonging to the pathway and R the fraction of pathway neurons included in the community; for each partition the community with the largest F_1 is taken.

Spatial attenuation by delay (shortest path through the network) as f was tried and rejected: such a function is built from the same connections as the graph itself, the null model reproduces the data, and $Q \to 0$ on sparse graphs.

Finally, to find out which properties of the network are created by growth, the results are compared with random networks built without growth from the same initial placement: the same neuron centres, initial axon ends, and number of dendrites of each

neuron. Each dendrite (except those of input neurons) is connected to a randomly chosen axon of another neuron, and its end is placed at the end of the chosen axon, so that the dendrite length equals the distance d from the neuron centre to the axon end. Dendrites are processed in random order, and the probability of choosing an axon is proportional to $K(d)/(1+n)$, where n is the number of dendrites already attached to it; the factor $1/(1+n)$ reproduces the limited axon capacity of the growth model. In variant R1, $K \equiv 1$ and all axons are equally likely. In variant R2, $K(d)$ is the probability that a dendrite connects to an axon end at distance d from the neuron centre, measured on grown networks of the same size: the ratio of the number of contacts to the number of pairs "neuron – end of another neuron's axon" in distance bins of width 0.02. This kernel is local: it halves by $d \approx 0.1$ and drops almost to zero by $d \approx 0.3$. Variant R2 thus reproduces the connection-length statistics of the grown network but without axon movement and without the dendrite growth field, whereas R1 is a network whose connections do not depend on distance at all. For each of the 30 grown networks one network of each variant is built, and all simulations are repeated on them.

4 Results

4.1 Grown networks

Simulations were performed on networks grown by the batch utility with the default growth parameters: 10 realizations (random seeds 1–10) for each of $N = 100$, 300 and 500 neurons, 6 of which are input and 6 output neurons. The network characteristics are listed in Table 1. The number of contacts grows in proportion to the number of neurons (about two per neuron), and the mean lengths of axons and dendrites hardly depend on network size. Almost all dendrites find an axon, and almost every axon is caught by at least one dendrite: the capacity limit prevents dendrites from gathering at a few axons. Practically the whole network is reachable from the inputs along the direction of connections. The exception is a few input neurons without outgoing connections: their signal never enters the network, whatever the weight.

The model parameters (Table A1 in Appendix A) are the same in all simulations. The basic input is periodic spikes with interval $T = 20$ ms applied to every dendrite of every input neuron from 10 to 1000 ms. The simulation lasts 2000 ms, so the second half shows what remains in the network after the signal stops.

4.2 Propagation threshold

Figure 2a shows how the fraction of fired neurons depends on the connection weight relative to the threshold w_c of the given network. At small weight only the input neurons fire. At a weight equal to the threshold about half of the network fires, with a large spread between realizations, and at a weight a quarter above the threshold practically the whole network fires. The transition from local activity to activation of the whole network occurs when the weight changes by less than a factor of one and a half, and the curves for different N almost coincide. Raster plots (Fig. 2c) show the same for a single network: below the threshold about a fifth of the neurons fire,

Table 1 Network characteristics (mean ± SD over 10 realizations)

	$N = 100$	$N = 300$	$N = 500$
contacts	184 ± 5	572 ± 13	971 ± 18
unconnected dendrites	3 ± 2	15 ± 9	15 ± 6
uncaught axons, %	4.3 ± 2.3	6.8 ± 1.2	7.4 ± 2.4
largest number of dendrites per axon	6	9	12
mean axon length L_a	0.61 ± 0.03	0.61 ± 0.03	0.60 ± 0.02
mean dendrite length L_d	0.17 ± 0.01	0.19 ± 0.01	0.20 ± 0.01
fraction reachable from inputs	1.00	0.98	0.99
inputs without outgoing connections, %	7	5	15
inputs from which outputs are reachable, %	93	95	85
threshold w_c	1.00 ± 0.03	1.07 ± 0.03	1.11 ± 0.03
runaway without depression, $w_0 \geq$	0.68 ± 0.05	0.70 ± 0.03	0.74 ± 0.06

forming a pathway through the whole depth of the domain; above it, practically the whole network fires. This transition is percolation-like, as in neuronal cultures (Breskin et al. 2006): when the fraction of connections able to conduct a spike exceeds a critical value, excitation spreads over the whole connected component.

The threshold itself hardly depends on network size (Table 1). It is determined by the mean degree, which in grown networks hardly depends on N, and by the dendrite length, since attenuation along the dendrite enters the connection weight (4). The small increase of the threshold with N is due to a slight lengthening of dendrites; we show below that in a network with long dendrites the threshold is twice as high.

Output neurons start to respond at the same point at which activity spreads over the network. There is no intermediate regime at uniform weight in which the signal reaches the outputs without exciting most of the network: the path from inputs to outputs passes through most of the network. A search for parameters at which "a spike reaches the output but does not excite the whole network" therefore reduces, at uniform weights, to choosing a point on the steep part of the transition.

4.3 Stability and transmitter depletion

Without transmitter depletion (Fig. 2b, d) the network switches to a self-sustained regime already at a weight of about two thirds of the threshold: excitation circulates through cycles of the network and does not stop after the input ends. The runaway does not start immediately. At first the network responds to the input locally, while passing spikes thicken connections (Fig. 2d). When the weight of the most used connections reaches the threshold, activity spreads over the network like an avalanche and then sustains itself, continuing to thicken the connections through which it circulates. Thickness plasticity thus acts as positive feedback, and without a mechanism that saturates transmission the model is unstable. Transmitter depletion (9) limits the transmitted weight, and after the input ends activity dies out within tens of milliseconds (Fig. 2c) in all simulations with weights up to $1.1\, w_c$.

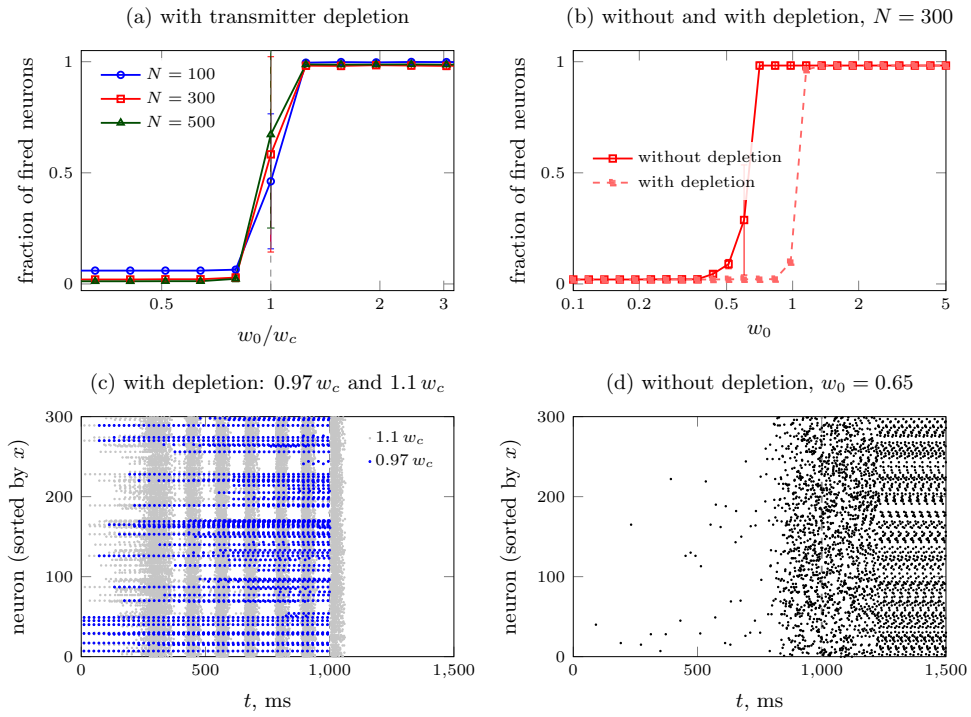
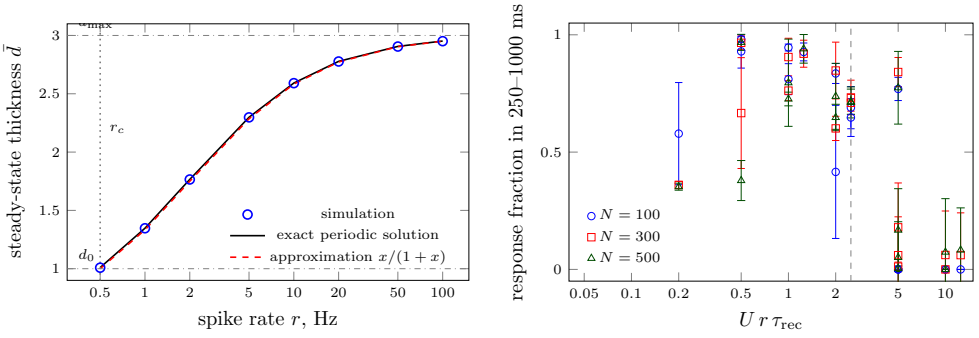


Fig. 2 Propagation regimes; all inputs, $T = 20$ ms. (a) Fraction of fired neurons versus w_0/w_c, with transmitter depletion; mean and SD over networks, vertical line $w_0 = w_c$. (b) The same fraction versus w_0 without depletion (solid) and with it (dashed), $N = 300$. (c) Raster plots of an $N = 300$ network at $0.97\,w_c$ (blue) and $1.1\,w_c$ (grey); neurons are sorted by x, the dashed line marks the end of stimulation. (d) The same without depletion, $w_0 = 0.65$.

Both runaway activity and pathway extraction rely on the thickening of connections. The steady-state thickness under periodic spiking obtained in the simulation coincides with the exact solution (6) over the whole frequency range, and the approximation (7) is close to it (Fig. 3a). Below the rate threshold (8) a connection does not thicken, but already at a few hertz its thickness is close to the maximum. Therefore, with $\tau_D = 10$ s, practically any connection through which spikes pass regularly thickens almost to the maximum, and pathways differ primarily in whether the signal passes through a connection at all, rather than in its rate.

Transmitter depletion also determines whether the network transmits the signal during the whole stimulation or only at its onset. Figure 3b shows the response fraction, the fraction of spikes of non-input neurons that fall in the interval 250–1000 ms (the middle and end of stimulation) among all their spikes, for $U = 0.02$–0.2 and input intervals $T = 2$–50 ms at weight $1.1\,w_c$ (the threshold w_c was found separately for each pair U, T). Points for different U and T group by the dimensionless synaptic load $Ur\tau_{\text{rec}}$, where $r = 1/T$. At low load the network works as a relay and transmits the signal during the whole stimulation. At high load it works as an onset detector:



(a) (b)

Fig. 3 (a) Steady-state thickness $\bar{d}$ versus spike rate r: simulation (points), exact solution (6) (solid) and approximation (7) (dashed); the vertical line is the threshold r_c (8). (b) Response fraction in 250–1000 ms versus synaptic load $Ur\tau_{\mathrm{rec}}$, $w_0 = 1.1\,w_c$; mean and SD over networks.

the first spikes pass while the resource is not depleted, and then the weight $w\,R^* \approx w/(1 + Ur\tau_{\mathrm{rec}})$ becomes insufficient for firing. The boundary lies between loads of 2.5 and 5. At the weakest depression ($U = 0.02$) the boundary is blurred because the network is close to the self-sustained regime. The baseline values $U = 0.05$ and $T = 20$ ms correspond to a load of 1.25 and ensure stable transmission. With $U = 0.6$, typical of cortical synapses (Tsodyks and Markram 1997), the network would be an onset detector for any $T \leq 50$ ms, and the signal trace would be confined to the vicinity of the inputs.

4.4 Signal pathway and comparison of stimuli

Thus, at a weight slightly below the threshold, the signal spreads over part of the network and thickens the connections it has passed through, and with $\tau_D = 10$ s this trace persists for seconds after the stimulation ends. We now extract this trace, the signal pathway, and compare pathways for different stimuli. Pathways were determined at $w_0 = 0.97\,w_c$ for eight stimuli: all inputs with intervals of 10, 20 and 50 ms; input triplets 0–2 and 3–5 ($T = 20$ ms); single inputs 0 and 5; and a Poisson signal with a mean rate of 50 Hz on all inputs. Each simulation starts from the initial thicknesses. Pathway sizes are given in Table 2.

When all inputs are stimulated, the pathway covers from a third to a half of the network. It contains only slightly more edges than neurons, i.e., the pathway is close to a tree branching from the inputs. The pathway contains all fired neurons and, in addition, a considerable fraction of neurons that did not fire: the signal reached them and thickened their dendrites but did not bring them to threshold. The pathway reaches only one or two of the six output neurons.

The pathway size depends on the temporal structure of the signal. With frequent input (10 ms) the pathway is shorter than with 20 ms because the connections become depleted. A Poisson signal with the same mean rate creates a pathway about twice as large as the periodic one: short intervals in the Poisson train summate on the membrane and bring to threshold neurons that do not fire under regular input. The

Table 2 Number of neurons in the signal pathway at $w_0 = 0.97\,w_c$ (mean ± SD over networks)

stimulus	$N = 100$	$N = 300$	$N = 500$
all inputs, 10 ms	31 ± 9	58 ± 19	70 ± 19
all inputs, 20 ms	46 ± 8	113 ± 18	155 ± 41
all inputs, 50 ms	47 ± 7	80 ± 19	84 ± 25
inputs 0–2	23 ± 9	62 ± 32	62 ± 28
inputs 3–5	25 ± 10	57 ± 23	97 ± 43
input 0	5 ± 4	18 ± 22	11 ± 11
input 5	8 ± 6	17 ± 21	23 ± 26
Poisson, 50 Hz	86 ± 8	221 ± 24	331 ± 38

pathway from a single input is small and varies strongly from network to network: the neighbours of an input neuron usually need summation of several inputs to fire.

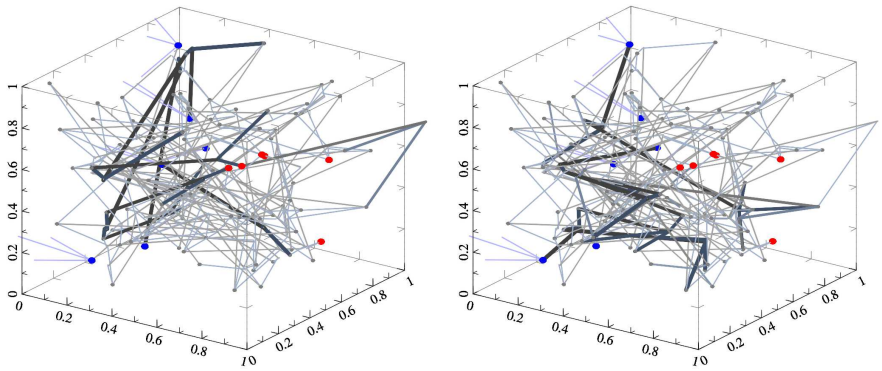
An example of pathways from two different input triplets in the same network is shown in Fig. 4. Below the threshold the pathways start from different input neurons and hardly overlap, and the thickened connections form elongated chains rather than compact groups. Above the threshold the pathways grow, reach all outputs and largely coincide: the signal spreads over almost the whole network, and the trace of the stimulus is blurred.

The network-averaged matrices of pathway comparison (Fig. 5) show the same picture. Stimuli on all inputs with different intervals, including the Poisson one, produce similar pathways. Pathways from disjoint groups of inputs practically do not coincide, and the pathway of a single input is contained in the pathway of the triplet that includes it: nested stimuli produce nested pathways. The correlation r_g is always higher than the Jaccard index J_N because it also accounts for connections that thickened less than the threshold g_0, and it therefore distinguishes stimuli more smoothly. Above the transition threshold, stimuli on all inputs cover practically the whole network and are indistinguishable; differences remain only for subsets of inputs. Stimuli can thus be distinguished by their trace in the network only below the threshold.

4.5 Community detection

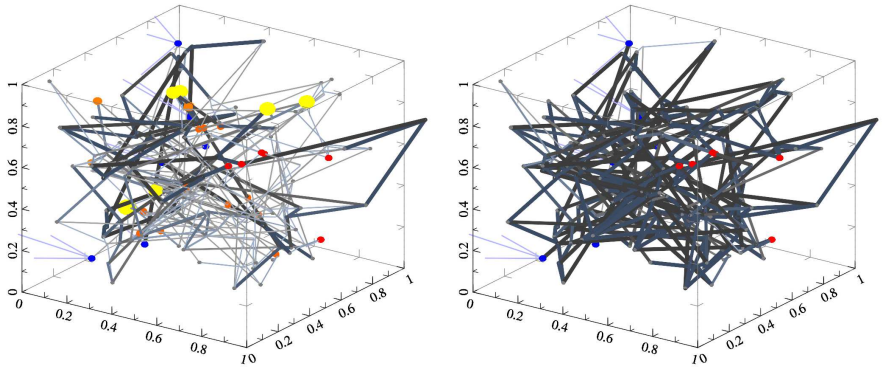
Here the signal pathway is extracted directly, from weight growth and reachability from the inputs. It is natural to ask whether standard community detection also finds it. To check this, the Louvain method with the normalized spatial null model (10) was applied to the graph after a simulation with stimulation of all inputs ($T = 20$ ms, $0.97\,w_c$), with weights S, A, A/A_0, $(A/A_0)^2$ and C and $\gamma = 1$, 0.3 and 0.1 (20 runs each; the partition with the largest Q is taken). For each partition we found the community that best matches the pathway and its F_1 score.

The weight variants differ in the information about the signal they carry. The structural weight depends only on the lengths of the axon and the dendrite and not on the signal; it serves as a control and shows what community detection gives without any information about the signal. The weight after the simulation and its growth



(a) inputs 0–2, $w_0 = 0.97\,w_c$

(b) inputs 3–5, $w_0 = 0.97\,w_c$



(c) inputs 0–2, $w_0 = 1.1\,w_c$

(d) inputs 3–5, $w_0 = 1.1\,w_c$

Fig. 4 Signal pathways in an $N = 100$ network from inputs 0–2 (a, c) and 3–5 (b, d) at $w_0 = 0.97\,w_c$ (a, b) and $1.1\,w_c$ (c, d), time 1000 ms. Line width is proportional to the thickness of the axon or dendrite. Blue dots are input neurons, red dots output neurons; yellow spheres are firing neurons, orange dots spikes in transit along axons and dendrites, red squares spikes arriving at the axon ends of output neurons.

during the simulation reflect the thickening of connections, and the pathway itself is extracted from the weight growth; the squared growth separates thickened connections from the rest even more strongly. The causal transmission weight is the number of times a neuron fired following a spike of another neuron; it reflects the activity itself rather than the change in thickness. The F_1 score takes into account both the fraction of community neurons that belong to the pathway and the fraction of pathway neurons that fall into the community: it equals one if the community coincides with the pathway and is close to zero if they hardly overlap.

None of the weights recovers the pathway (Fig. 6a, b): the best community matches the pathway by at most a third, and the match deteriorates as the network grows. Weights that account for the growth of connections are only slightly better than the structural weight, which does not depend on the signal. The causal transmission weight C gives the highest modularity but splits the network into communities of one or two neurons. Decreasing γ makes communities coarser and slightly improves the match but does not change the conclusion. At the same time, the modularity of the partitions

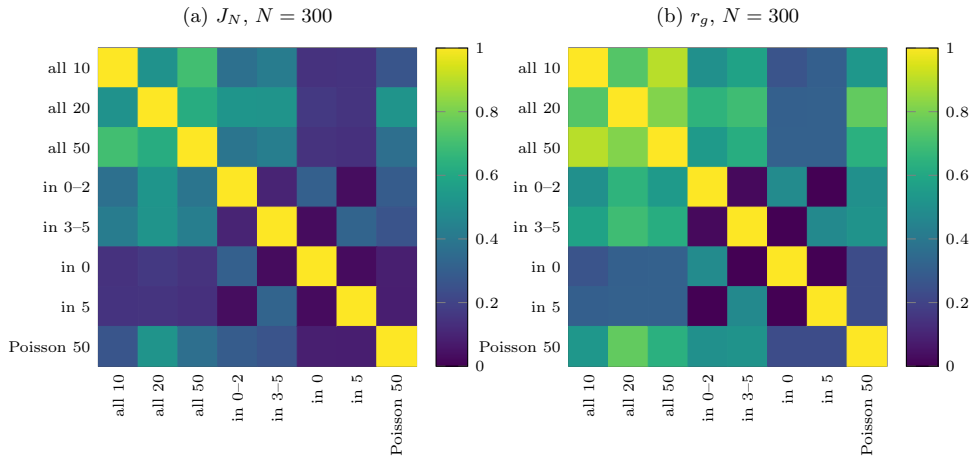


Fig. 5 Pairwise comparison of pathways for the eight stimuli of Table 2, $N = 300$, $w_0 = 0.97\,w_c$, mean over 10 networks: (a) Jaccard index J_N; (b) correlation r_g of weight growth.

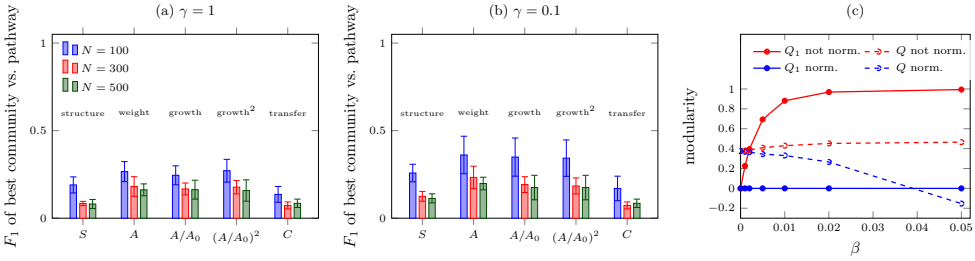


Fig. 6 (a, b) F_1 score of the Louvain community that best matches the signal pathway, for different connection weights at $\gamma = 1$ (a) and $\gamma = 0.1$ (b); mean and SD over networks. The horizontal axis shows the weight variant: structural (S), after the simulation (A), its growth (A/A_0) and squared growth, causal transmission (C). (c) Modularity of the trivial partition Q_1 (solid) and of the partition found Q (dashed) versus β without normalization of the null model (red) and with it (blue), $N = 300$.

found is high, so a high Q by itself does not mean that the communities reflect the signal pathway.

We also checked the effect of normalizing the null model (Fig. 6c; coordinates, as in Trubitsin 2026, in units of a domain of size 400). Without normalization, the modularity of the trivial partition "the whole network is one community", which by definition should be zero, grows with β almost to one: the expected weight $\sum P_{ij}$ becomes much smaller than m, and any group of connected neurons looks "denser than expected". With normalization the modularity of the trivial partition is zero for all β, and the modularity of the partition found decreases with β and becomes negative. The growth of Q with β in the unnormalized model is thus entirely an artefact. Under strong attenuation the null model expects mostly short connections,

whereas the connections of the grown network are not shorter than random ones (see below), so no communities beyond spatial proximity are found.

4.6 Role of growth

The remaining question is which of the results are due to growth as such. To answer it, the grown networks were compared with the random networks R1 and R2 (Section 3) built without growth from the same initial placement. Distributions of the characteristics of all three networks are shown in Fig. 7, and a summary is given in Table 3.

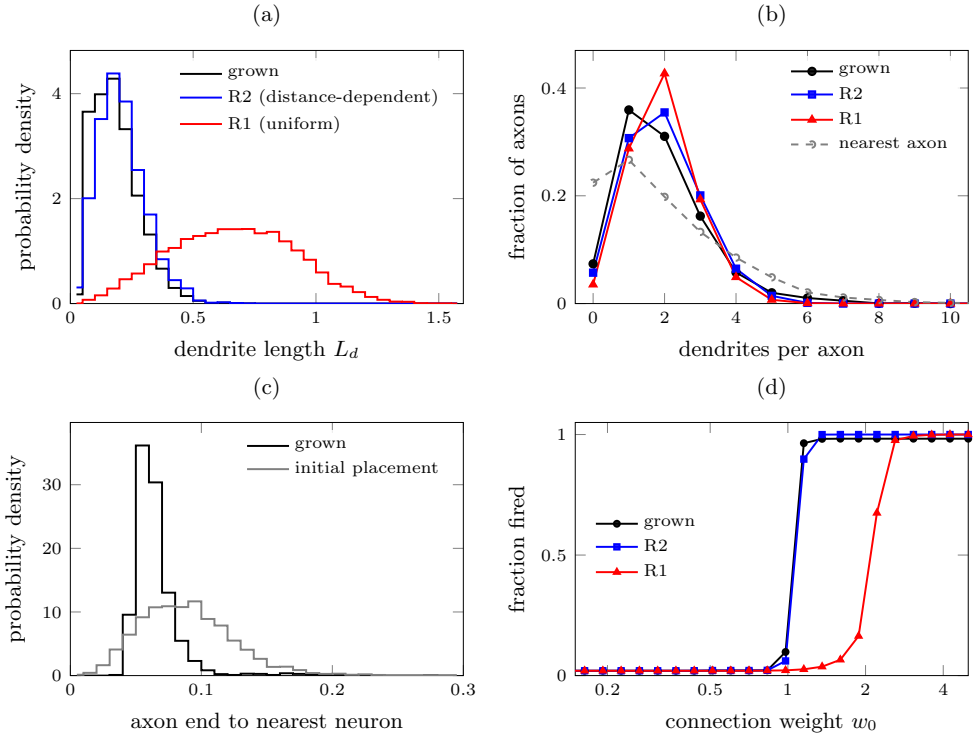


Fig. 7 Grown network (G) and random networks R1 and R2, $N = 300$, 10 realizations. (a) Dendrite length. (b) Number of dendrites per axon; the dashed line corresponds to connection to the nearest axon without the capacity limit. (c) Distance from an axon end to the nearest neuron of another cell. (d) Fraction of fired neurons versus w_0.

Axon growth markedly changes the placement of axons (Fig. 7c). During growth an axon end moves by about a third of the mean axon length and stops near some neuron at an almost constant distance, where attraction to the neuron is balanced by repulsion from it. Axon ends also move apart from each other and away from the domain boundaries; in the initial placement the same distances are spread 2–3 times

Table 3 Grown networks (G) and random networks without growth: R2 — distance-dependent connections as in grown networks, R1 — uniform; mean over 10 realizations, SD in parentheses. E is the total energy (1); pathway, outputs and F_1 refer to the stimulus "all inputs, 20 ms", $w_0 = 0.97\, w_c$; F_1 for weight A, $\gamma = 0.1$; J_N for pathways from inputs 0–2 and 3–5.

	network	$N = 100$	$N = 300$	$N = 500$
total energy E	G	1299 (107)	3031 (186)	4647 (287)
	R1, R2	550 (32)	1706 (50)	2869 (67)
dendrite length L_d	G	0.17	0.19	0.20
	R2	0.23	0.21	0.21
	R1	0.67	0.66	0.66
axons without dendrites, %	G	7	7	8
	R2	10	6	5
	R1	5	4	3
threshold w_c	G	1.00 (0.03)	1.07 (0.03)	1.11 (0.03)
	R2	1.14 (0.06)	1.11 (0.01)	1.13 (0.01)
	R1	2.08 (0.19)	2.13 (0.10)	2.19 (0.06)
runaway without depression,	G	0.67	0.65	0.67
$w_0/w_c \geq$	R2	0.63	0.64	0.69
	R1	0.61	0.63	0.61
neurons in pathway	G	46	113	155
	R2	44	110	161
	R1	58	161	260
outputs reached	G	1.8	0.9	1.7
	R2	2.3	1.3	2.2
	R1	3.1	3.3	2.7
J_N of pathways from different inputs	G	0.16	0.10	0.10
	R2	0.10	0.10	0.07
	R1	0.18	0.19	0.19
F_1 of community and pathway	G	0.36	0.23	0.20
	R2	0.34	0.24	0.16
	R1	0.32	0.16	0.12

more widely. The total energy (1) increases during growth by a factor of 1.6–2.4, mainly due to the field of the neurons near which axon ends gather.

Growth, however, does not change the distance between the centres of connected neurons: it is the same as between two random points of the cube. An axon starts at a random point and reaches the neuron nearest to it, so the connection range is set by the initial position of the axon end.

Dendrite growth determines which axons the dendrites connect to. A dendrite catches an axon whose end is close to its neuron, and dendrites turn out short (Fig. 7a). In network R2 they are only slightly longer, and in R1, where connections do not depend on distance, three times longer. The distribution of the number of dendrites per axon is similar in the grown network and in both random networks (Fig. 7b), since

the capacity limit acts in all three. Without it, if each dendrite connects to the nearest axon, about a quarter of the axons remain uncaught, and individual axons collect more than ten dendrites. In the grown network the tail of the distribution is somewhat longer: axon ends gathered near one neuron are caught by its dendrites together.

The signal propagates in network R2 almost as in the grown network (Table 3). Its threshold is only slightly higher because of somewhat longer dendrites, and the pathway size, the number of outputs reached, the overlap of pathways from different inputs and the match with Louvain communities agree within the spread between networks.

Network R1 behaves differently. Long dendrites attenuate the connection weight more strongly (4), and the threshold is twice as high (Fig. 7d). At the same relative weight the signal pathway is larger and reaches the outputs more often, and pathways from different groups of inputs overlap twice as strongly; pathways from single inputs grow particularly large. Without spatial locality the signal from an input spreads into different parts of the network, and the traces of different stimuli mix. The Louvain method recovers the pathway in R1 even worse. The modularity of the partition by structural weight is the same in all three networks; any sparse random graph has the same modularity (Guimerà et al. 2004), so the communities in the grown network do not reflect structure beyond that of a random graph.

5 Discussion

The main feature of the model, thickness plasticity, acts as positive feedback: a passing signal thickens and speeds up a connection, which facilitates the passage of the next signal. Without a limiter this leads to runaway activity, and not immediately but after a kind of "training" of the network (Fig. 2d). An upper bound on thickness ($d_{\max}$) does not by itself save the network: the maximum weight $w_0 d_{\max}/d_0$ is three times the initial one. The network is stabilized by transmitter depletion, which limits the weight flux through a contact to $w/(U\tau_{\mathrm{rec}})$. The strength of depletion also selects the operating regime of the network: the boundary between the relay and the onset detector is set by a single dimensionless quantity, $Ur\tau_{\mathrm{rec}} \approx 2.5$–$5$ (Fig. 3b). This agrees with the analysis of networks with depressing synapses (Tsodyks et al. 1998), where resource depletion determines whether the network responds to input steadily or with brief synchronous bursts. In the models of Talidou et al. (2022); Lefebvre et al. (2025), where myelin affects only the delays, it acts as a gain control mechanism that stabilizes network dynamics; in our model thickness also enters the connection weight, and plasticity becomes positive feedback that requires a limiter. The onset-detector regime is akin to the effect in which short-term depression weakens the response to a frequently repeated stimulus near the stimulation site (Kern and Chao 2023). Inhibitory neurons could serve as another limiter; the program supports them (fraction p_{inh} and factor g), but they were not used in this work in order not to mix the two mechanisms.

Once the network is stable, signal propagation is governed by the connection weight, and the transition from a local response to activation of the whole network turns out to be sharp. There is no regime at uniform weight in which the signal reaches the outputs without spreading over the network, which is natural for a percolation

transition in a random spatial network: below the threshold the signal dies out a few connections away from the input, above it the signal spreads over the connected component. Such a regime is possible only with non-uniform weights, when the path to the outputs is formed by connections stronger than average. This is exactly the kind of non-uniformity created by thickness plasticity: below the threshold ($0.97\,w_c$), repeated stimulation thickens the connections through which the signal has already passed and thereby singles out its pathway. This is a mechanism of memory of the stimulus with a retention time of order τ_D.

A comparison of such pathways shows what exactly the network remembers. The proposed measures make it possible to compare the changes caused by different signals without community detection: the Jaccard indices answer whether the same neurons and connections form the pathway, and the correlation r_g whether the changes of the network as a whole are consistent. Pathways from different inputs are separated, nested stimuli produce nested pathways, and the temporal structure of the signal (period, Poisson train) changes the pathway size while its composition stays similar. The signal trace in connection thicknesses thus carries information primarily about *where* the signal came from, and to a lesser extent about its temporal structure.

Standard community detection does not find this trace, and the reason lies in the nature of modularity itself. Modularity compares the density of connections within a group with the expected one and rewards groups with many internal and few external connections. The signal pathway is organized differently: it is almost a tree (with only 4–10 % more edges than nodes), stretched from inputs to outputs across the whole domain, and each pathway node is also connected to neurons outside it. The growth of connection weight along the pathway is bounded by the ratio $d_{\max}/d_0 = 3$ (9 for $(A/A_0)^2$), which is not enough to outweigh the numerous external connections, and the spatial null model shifts communities even further towards compact groups of neighbours. The signal pathway is an object of a different kind than a community and should be extracted directly, from weight growth and reachability from the inputs, as proposed here; modularity is useful for describing the structure of the network but not the trace of a signal.

All these properties were obtained on grown networks, and the comparison with random networks shows that growth affects them through the spatial locality of connections with respect to axon ends. Axon growth gathers axon ends near neurons (the total energy increases by a factor of 1.6–2.4), dendrite growth connects each dendrite to a nearby axon end, and dendrites turn out short. This gives a low transition threshold, a small overlap of pathways from different inputs, and sensitivity of the pathway to the temporal structure of the signal. A network whose connections do not depend on distance (R1) has a twice higher threshold and mixes the traces of different stimuli more strongly. At the same time, all functional properties of the grown network are reproduced by the random network R2 built from two rules: the probability that a dendrite connects to an axon decays with the distance from the neuron to the axon end according to the measured kernel $K(d)$, and an occupied axon is less attractive. Connectome generative models show that simple geometric rules reproduce the structure of brain networks (Liu et al. 2024; Richter and Schneidman 2025); our result complements this with the functional side: rule R2 reproduces signal propagation as

well. The energy of R2 is the same as that of the initial placement, since it describes the positions of axon ends rather than who is connected to whom. Growth does not change the connection range between neurons (0.66, as for random points): it is set by the initial random position of the axon end. If the initial axon end were placed close to its own neuron, the axon length, and with it the connection range, would be determined by growth itself; this is a natural extension of the model.

The conclusions should be considered in light of the limitations of the model. The neuron model is the simplest one (LIF without adaptation), the synapse is purely depressing, and axon thickness changes at every firing of the neuron regardless of whether the spike reached the contact. The network is small (up to 500 neurons). The connectivity of the grown network depends substantially on the growth rules: without the axon capacity limit, dendrites gather at a few axons, and for $N = 300$–500 up to a third of the neurons (including input ones) do not pass the signal on. The capacity limit largely removes this problem, but 5–15 % of inputs still have no outgoing connections. The random networks are built from the initial placement and differ from the grown network both in the positions of axon ends and in the connection rule; these two contributions can be separated by applying the rules of R1 and R2 to grown axons. The thinning time $\tau_D = 10$ s, as in other models of myelin plasticity (Nguyen and Lefebvre 2026), is much shorter than the real time of myelin remodelling (hours to days): time is compressed so that the signal trace is visible in a short simulation. Finally, the simulations cover 1–2 s of model time, whereas $\tau_D = 10$ s, and the behaviour under repeated changes of stimuli and competition between pathways remains a subject for future work.

6 Conclusion

We proposed a model of spike propagation in a self-organized three-dimensional neural network in which the delay and weight of a connection are determined by the length and thickness of the axon and dendrite, and thickness changes with passing spikes. The exact steady-state thickness under periodic spiking and the rate threshold (8) above which a connection thickens were derived; the simulations agree with them to within 10^{-3}.

On 30 grown networks of 100–500 neurons we showed that signal propagation has a sharp threshold in connection weight, $w_c \approx 1.0$–1.1, which depends only weakly on network size, and that without short-term depression thickness plasticity leads to self-sustained activity already at $w_0 \approx 0.7\, w_c$. The strength of depression, through the quantity $Ur\tau_{\mathrm{rec}}$, determines whether the network works as a relay ($\lesssim 2.5$) or as an onset detector ($\gtrsim 5$).

We proposed a method for extracting the signal pathway from the growth of connection weights and reachability from the inputs, together with measures for comparing pathways. Pathways from different groups of inputs practically do not overlap, pathways of nested stimuli are nested, and stimuli remain distinguishable only below the transition threshold. Community detection by the Louvain method does not recover the signal pathway with any of the weights considered ($F_1 \leq 0.36$), because

the pathway is an elongated tree rather than a dense group. We showed that the spatial null model of modularity without normalization overestimates modularity, up to $Q \approx 1$ for the trivial partition, so normalization is necessary.

A comparison with random networks built without growth from the same initial placement showed that growth increases the total energy of the network by a factor of 1.6–2.4 by gathering axon ends near neurons, and connects dendrites to nearby axons. A network in which connections do not depend on distance has a twice higher transition threshold and mixes pathways from different inputs more strongly. A random network with connection probability decaying with distance according to the kernel measured on grown networks, and with a limited axon capacity, reproduces all functional properties of the grown network.

The simulation program and the batch utility are part of the NNBiology package.

Acknowledgements.

Statements and Declarations

- **Funding.** The state assignment of the Ministry of Science and Higher Education of the Russian Federation, project No. . . . 125020501424-2.
- **Competing interests.** The author has no relevant financial or non-financial interests to disclose.
- **Ethics approval and consent.** Not applicable: the study is purely computational and involves no human participants or animals.
- **Data availability.** The data generated in this study are available from the corresponding author on reasonable request.
- **Code availability.** The simulation code is part of the NNBiology software package (C++, Qt); it can be obtained reasonable request.
- **Author contributions.** V. Yu. Trubitsin is the sole author and carried out the conceptualization, model development, software, simulations, analysis and writing.
- **Use of generative AI.** During the preparation of this work the author used Claude (Anthropic) to assist with translation into English, text editing and preparation of figures. The author reviewed and edited all content and takes full responsibility for the publication."

Appendix A Model parameters

The parameters common to all simulations are listed in Table A1.

Appendix B Numerical values for Section 4

Tables B2 and B3 collect the numerical values on which the text of Section 4 relies and which are not directly visible in the figures and tables. Unless stated otherwise, the values are means over 10 realizations for $N = 100$, 300 and 500 (separated by slashes) or a range over N.

Table A1 Model parameters used in the simulations

Neuron		
time step, simulation length	Δt, t_{sim}	0.1 ms, 2000 ms
leak time constant	τ_m	5 ms
threshold, rest, reset	θ, V_{rest}, V_{reset}	1, 0, 0
refractory period	t_{ref}	2 ms
Connection		
domain size	L_{dom}	1 mm
synaptic delay	t_{syn}	0.5 ms
dendrite length constant	λ_0	0.5
connection weight	w_0	$0.97\,w_c$ or $1.1\,w_c$
Thickness (axon / dendrite)		
initial, minimum, maximum	d_0, d_{min}, d_{max}	1, 0.5, 3
increment per spike	η	0.05
thinning time	τ_D	10 s
velocity at d_0	v_0	1 / 0.2 L_{dom}/ms
exponent	β	1 / 0.5
update of delays and weights	N_{upd}	100 steps
Depression		
fraction of resource used	U	0.05
recovery time	τ_{rec}	500 ms
Input		
weight of external spike	$w_{0,\mathrm{in}}$	5
interval, stimulation period	T	20 ms, 10–1000 ms
thickness of input dendrites		fixed

Table B2 Numerical values for Section 4

Grown networks (Table 1)	
contacts per neuron	≈ 1.9
unconnected dendrites, %	1.5–3
Threshold (Fig. 2)	
fraction fired at $w_0 < 0.65\, w_c$	$6/N$ (inputs only)
at $0.8\, w_c$; w_c; $1.25\, w_c$	2–6 %; 46–67 %; 98–99.6 %
fraction of outputs responding at $0.8\, w_c$; w_c; $1.25\, w_c$	0; 32–60 %; 95–100 %
attenuation e^{-L_d/λ_0} at $L_d = 0.17$ and 0.20	0.71 and 0.67
runaway without depletion, w_0	0.68–0.74 ($\approx 0.68\, w_c$)
Thickness and transmitter depletion (Fig. 3)	
deviation of simulation from solution (6), 0.5–100 Hz	$< 10^{-3}$
deviation of approximation (7) from exact solution	≤ 0.015
$\bar{d}$ at 0.5; 5; 20 Hz	1.01; 2.3; 2.78
response fraction in 250–1000 ms at $Ur\tau_{\rm rec} \leq 2.5$	0.42–0.97 (mostly > 0.7)
at $Ur\tau_{\rm rec} \geq 5$	≤ 0.18
at $U = 0.02$, $T = 50$ ms	0.35–0.58
Signal pathway (Table 2, Figs. 4, 5), $0.97\, w_c$	
edges in pathway, all inputs, 20 ms	48 / 123 / 170
fraction of non-fired neurons in pathway	≈ 40 %
F_1 of pathway and set of fired neurons	0.75–0.77
Poisson pathway / periodic (20 ms)	1.9–2.1
example of Fig. 4: neurons in pathways, J_N, $0.97\, w_c$	19 and 33; 0.04
the same at $1.1\, w_c$	74 and 97; 0.71
J_N, r_g ($N = 300$): all inputs, different intervals	0.51–0.70; 0.73–0.89
Poisson and 20 ms	0.52; 0.76
inputs 0–2 and 3–5	0.10; 0.02
input 0 and input 5	0.03; 0.00
input 0 and inputs 0–2; input 5 and inputs 3–5	0.30; 0.48 and 0.32; 0.47
neurons in pathway at $1.1\, w_c$, all inputs, $N = 300$	286–294

Table B3 Numerical values for Section 4 (continued)

Community detection (Fig. 6)	
largest F_1 (weight A, $\gamma = 0.1$)	0.36 / 0.23 / 0.20
F_1 for structural weight S	0.08–0.26
weight C: Q; number of communities	0.4–0.9; 93 / 280 / 466
F_1 for weight C	≤ 0.17
modularity of partitions found	0.4–0.7
without normalization, $N = 300$: Q_1 at $\beta = 0.001$; 0.01; 0.05	0.23; 0.88; 0.99
Q of partition found	from 0.37 to 0.47
with normalization: Q at $\beta = 0$; 0.01; 0.02; 0.05	0.37; 0.33; 0.27; -0.15
Role of growth (Fig. 7, Table 3)	
displacement of axon end during growth	0.22
distance from axon end to neuron: grown; initial	0.05–0.09; 0.09–0.14
distance between neighbouring axon ends	0.07–0.10
distance between centres of connected neurons	0.64–0.67 (random points: 0.66)
connection to nearest axon without capacity limit: uncaught axons; largest number of dendrites per axon	21–29 %; 14
neurons in pathways from inputs 0 and 5, $N = 500$: grown; R1	11 and 23; 77 and 51
J_N of pathways from all inputs at 10 and 50 ms, $N = 300$–500: grown; R1	0.67–0.70; 0.39–0.49

References

Abbott LF, Varela JA, Sen K, et al (1997) Synaptic depression and cortical gain control. Science 275(5297):221–224. https://doi.org/10.1126/science.275.5297.221

Betzel RF, Medaglia JD, Papadopoulos L, et al (2017) The modular organization of human anatomical brain networks: accounting for the cost of wiring. Network Neuroscience 1(1):42–68. https://doi.org/10.1162/NETN_a_00002

Blondel VD, Guillaume JL, Lambiotte R, et al (2008) Fast unfolding of communities in large networks. Journal of Statistical Mechanics: Theory and Experiment 2008:P10008. https://doi.org/10.1088/1742-5468/2008/10/P10008

Bonetto G, Belin D, Káradóttir RT (2021) Myelin: a gatekeeper of activity-dependent circuit plasticity? Science 374(6569):eaba6905. https://doi.org/10.1126/science.aba6905

Breskin I, Soriano J, Moses E, et al (2006) Percolation in living neural networks. Physical Review Letters 97:188102. https://doi.org/10.1103/PhysRevLett.97.188102

Burkitt AN (2006) A review of the integrate-and-fire neuron model: I. Homogeneous synaptic input. Biological Cybernetics 95(1):1–19. https://doi.org/10.1007/s00422-006-0068-6

Butz M, Wörgötter F, van Ooyen A (2009) Activity-dependent structural plasticity. Brain Research Reviews 60(2):287–305. https://doi.org/10.1016/j.brainresrev.2008.12.023

Expert P, Evans TS, Blondel VD, et al (2011) Uncovering space-independent communities in spatial networks. Proceedings of the National Academy of Sciences of the USA 108(19):7663–7668. https://doi.org/10.1073/pnas.1018962108

Fields RD (2015) A new mechanism of nervous system plasticity: activity-dependent myelination. Nature Reviews Neuroscience 16(12):756–767. https://doi.org/10.1038/nrn4023

Fortunato S (2010) Community detection in graphs. Physics Reports 486(3–5):75–174. https://doi.org/10.1016/j.physrep.2009.11.002

Gast R, Knösche TR, Schmidt H (2021) Mean-field approximations of networks of spiking neurons with short-term synaptic plasticity. Physical Review E 104:044310. https://doi.org/10.1103/PhysRevE.104.044310

Gerstner W, Kistler WM (2002) Spiking Neuron Models. Cambridge University Press, Cambridge, https://doi.org/10.1017/CBO9780511815706

Gibson EM, Purger D, Mount CW, et al (2014) Neuronal activity promotes oligodendrogenesis and adaptive myelination in the mammalian brain. Science

344(6183):1252304. https://doi.org/10.1126/science.1252304

Guimerà R, Sales-Pardo M, Amaral LAN (2004) Modularity from fluctuations in random graphs and complex networks. Physical Review E 70:025101. https://doi.org/10.1103/PhysRevE.70.025101

Hebb DO (1949) The Organization of Behavior. Wiley, New York

Humphries MD (2011) Spike-train communities: finding groups of similar spike trains. Journal of Neuroscience 31(6):2321–2336. https://doi.org/10.1523/JNEUROSCI.2853-10.2011

Hursh JB (1939) Conduction velocity and diameter of nerve fibers. American Journal of Physiology 127(1):131–139. https://doi.org/10.1152/ajplegacy.1939.127.1.131

Izhikevich EM (2006) Polychronization: computation with spikes. Neural Computation 18(2):245–282. https://doi.org/10.1162/089976606775093882

Jaccard P (1912) The distribution of the flora in the alpine zone. New Phytologist 11(2):37–50. https://doi.org/10.1111/j.1469-8137.1912.tb05611.x

Kern FB, Chao ZC (2023) Short-term neuronal and synaptic plasticity act in synergy for deviance detection in spiking networks. PLOS Computational Biology 19(10):e1011554. https://doi.org/10.1371/journal.pcbi.1011554

Lefebvre J, Clappison A, Longtin A, et al (2025) Myelin-induced gain control in nonlinear neural networks. Communications Physics 8:145. https://doi.org/10.1038/s42005-025-02055-8

Leicht EA, Newman MEJ (2008) Community structure in directed networks. Physical Review Letters 100:118703. https://doi.org/10.1103/PhysRevLett.100.118703

Litwin-Kumar A, Doiron B (2014) Formation and maintenance of neuronal assemblies through synaptic plasticity. Nature Communications 5:5319. https://doi.org/10.1038/ncomms6319

Liu Y, Seguin C, Betzel RF, et al (2024) A generative model of the connectome with dynamic axon growth. Network Neuroscience 8(4):1192–1211. https://doi.org/10.1162/netn_a_00397

Newman MEJ, Girvan M (2004) Finding and evaluating community structure in networks. Physical Review E 69:026113. https://doi.org/10.1103/PhysRevE.69.026113

Nguyen T, Lefebvre J (2026) A computational roadmap to activity-dependent myelination. Frontiers in Computational Neuroscience 20:1895171. https://doi.org/10.3389/fncom.2026.1895171

Noori R, Park D, Griffiths JD, et al (2020) Activity-dependent myelination: a glial mechanism of oscillatory self-organization in large-scale brain networks. Proceedings of the National Academy of Sciences of the USA 117(24):13227–13237. https://doi.org/10.1073/pnas.1916646117

Pajevic S, Basser PJ, Fields RD (2014) Role of myelin plasticity in oscillations and synchrony of neuronal activity. Neuroscience 276:135–147. https://doi.org/10.1016/j.neuroscience.2013.11.007

Pajevic S, Plenz D, Basser PJ, et al (2023) Oligodendrocyte-mediated myelin plasticity and its role in neural synchronization. eLife 12:e81982. https://doi.org/10.7554/eLife.81982

Rall W (1962) Theory of physiological properties of dendrites. Annals of the New York Academy of Sciences 96(4):1071–1092. https://doi.org/10.1111/j.1749-6632.1962.tb54120.x

Reichardt J, Bornholdt S (2006) Statistical mechanics of community detection. Physical Review E 74:016110. https://doi.org/10.1103/PhysRevE.74.016110

Richter O, Schneidman E (2025) Building the connectome of a small brain with a simple stochastic developmental generative model. Proceedings of the National Academy of Sciences of the USA 122(47):e2504913122. https://doi.org/10.1073/pnas.2504913122

Rushton WAH (1951) A theory of the effects of fibre size in medullated nerve. Journal of Physiology 115(1):101–122. https://doi.org/10.1113/jphysiol.1951.sp004655

Shimono M, Beggs JM (2015) Functional clusters, hubs, and communities in the cortical microconnectome. Cerebral Cortex 25(10):3743–3757. https://doi.org/10.1093/cercor/bhu252

Talidou A, Frankland PW, Mabbott D, et al (2022) Homeostatic coordination and up-regulation of neural activity by activity-dependent myelination. Nature Computational Science 2(10):665–676. https://doi.org/10.1038/s43588-022-00315-z

Trubitsin VY (2026) Clustering of three-dimensional neural networks using the Louvain method. Khimicheskaya Fizika i Mezoskopiya (Chemical Physics and Mesoscopics) 28(3):389–397. https://doi.org/10.62669/17270227.2026.3.35, (in Russian)

Tsodyks M, Pawelzik K, Markram H (1998) Neural networks with dynamic synapses. Neural Computation 10(4):821–835. https://doi.org/10.1162/089976698300017502

Tsodyks MV, Markram H (1997) The neural code between neocortical pyramidal neurons depends on neurotransmitter release probability. Proceedings of the National Academy of Sciences of the USA 94(2):719–723. https://doi.org/10.1073/pnas.94.2.719

Supplementary Files

This is a list of supplementary files associated with this preprint. Click to download.

- CognNeurodynTrubitsinsubmission.zip